Journal of Research and Applications in Mechanical Engineering
ISSN: 2229-2152 (Print); 2697-424x (Online)
(2025) Vol. 13, No. 3, Paper No. JRAME 25-13-043
[DOI: 10.14456/ jrame.2025.43]

Research Article

In-plane Compression and Evolution Texture to Improve Drawability of Rolled AZ31B Magnesium-Alloy Sheets

M. Okawa[1,*]
T. Murakami[2]
T. Kuroki[1]
A. Takasaki[3]
[1] *Unit of Plastic Forming Engineering, Polytechnic University of Japan, Tokyo, 1870035, Japan*
[2] *Unit of Principles of Vocational Skills Development, Polytechnic University of Japan, Tokyo, 1870035, Japan*
[3] *Department of Engineering Science and Mechanics, Shibaura Institute of Technology, Tokyo, 1358548, Japan*

Received 30 August 2024
Revised 27 December 2024
Accepted 4 January 2025

Abstract:
Room-temperature forming of Mg alloy sheets is desirable over warm forming to mitigate machining hazards, lubricant degradation, and energy consumption. This study enhances the drawability of rolled Mg–3Al–1Zn (AZ31B) alloys at room temperature through in-plane compaction. Due to a limiting drawing ratio (LDR) below ~1.3, typical deep drawability parameters (n-value, r-value, tensile strength) could not be used. Instead, the activation of prism texture in surface sheets and the suppression of basal texture effectively accommodated thickness strain, improving drawability. In-plane pre-compression along angles relative to the rolling direction (RD) — 0° (RD), 30°, 45°, 60° and 90° (transverse directions, TDs) — with strains of 0.06 or 0.08 further enhanced formability. This process increased circumferential strain from 0.010 in as-received material to 0.227 in 6.0% pre-compressed specimens, demonstrating a significant improvement in room-temperature formability for AZ31B magnesium-alloy sheets.

Keywords: *Magnesium alloy sheet, Sheet metal, Forming, Drawing, In-plane compression test*

1. Introduction

Recently, room-temperature formable Mg-alloy sheets have been developed, prompting further research into their secondary formability [1]. However, press forming these sheets results in distinctive plastic deformation at room temperature, and an optimal processing method has yet to be established [2, 3]. Additionally, rolling induces a strong basal texture, which restricts sheet-thickness deformation and makes sheet forming challenging [4-9].

A recent method for controlling basal texture involves applying continuous bending strain in the out-of-plane direction [10]. While this approach produced a double-peak texture with excellent formability at room temperature (20–25 °C), maintenance was required at warmer temperatures to suppress crack generation under high pressure. Particularly, in deep drawing, the interpretation of the structure is more complex than that for other alloys, and deformation occurs at high temperatures, further complicating the process. Cylindrical deep drawing of rolled Mg–3Al–1Zn (AZ31B) Mg-alloy sheet was performed at room temperature, with the blank folder force varied to evaluate flange cracking, stress state, and microstructural changes [11].

Additionally, compressing an Mg-alloy rolled sheet in the in-plane direction generates fine waviness, enabling deformation in the sheet-thickness direction and thereby improving drawability [12-14].

Furthermore, drawability can be enhanced by tilting the *c*-axis of the grains to alter the overall basal texture or by activating {10-12} tension twins. However, it remains unclear which of these techniques plays a more significant role in improving press formability at room temperature.

* Corresponding author: M. Okawa
E-mail address: ookawa@uitec.ac.jp

This study investigated the effect of in-plane compression on the basal texture of Mg-alloy sheets through crystal-orientation analysis using X-ray diffraction (XRD) and electron backscattered diffraction (EBSD). Mg-alloy sheets were pre-strained via in-plane compression at angles of 0° (rolling direction (RD)), 30°, 45°, 60°, and 90° (transverse directions (TDs) from the RD, and their drawability was assessed. Furthermore, the in-plane compression conditions that most effectively enhance the drawability were identified.

2. Experimental Setup

This study employed an AZ31B Mg-alloy-rolled sheet (annealed at 360 °C for 1 h, with a nominal thickness t_0 = 1.0 mm) produced by NIPPON KINZOKU Co. Ltd., Japan. Figure 1 presents the (0001) pole figure (obtained via EBSD) and the microstructure (captured using an optical microscope). The basal texture of the hexagonal crystal is oriented parallel to the RD–TD plane, exhibiting a typical basal texture with a pole density of ≥11. The microstructure consists of spherical mixed grains with sizes ranging from 3 to 20 μm. A test specimen with an aspect ratio (λ) of 2 along the load axis and perpendicular directions was fabricated through wire electric discharge machining.

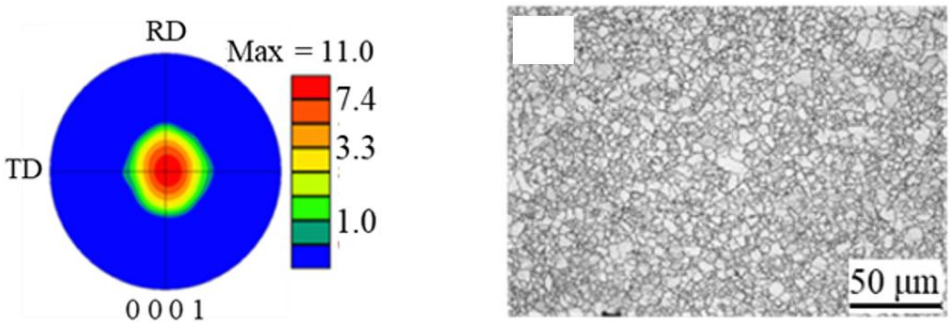

(a) (0001) pole figure obtained via EBSD (b) Photograph of the microstructure

Fig. 1. Characteristics of the as-received AZ31BMg alloy-rolled sheet.

Figure 2 illustrates a schematic of the test specimen, the in-plane compression apparatus, and its operation. The compression direction (θ) is represented as the angle relative to the RD, with 0° representing alignment between the two. The specimens were fabricated using compression angles of 0°, 30°, 45°, 60° and 90°. This activation enhances the behavior of the material, which was evaluated at different compression-direction angles (θ = 0°, 30°, 45°, 60° or 90°). These angles were selected to reproduce the stress state occurring during the forming process and evaluate the anisotropy of the material.

The in-plane compression apparatus was fabricated based on the in-plane reverse load-test apparatus employed by Kuwabara et al. [15]. It comprised a sheet holder with a pair of interlocking comb teeth and die. The specimen was held in place with a blank holder, with the holding pressure evenly applied at approximately 1.33 MPa (blank holder force (BHF) using bolts. The outermost specimen was cut to a diameter (φ) of 28 mm by a wire electric discharge machine. The initial strain rate for the in-plane compression test was set to 4.2 × 10–4s–1, and the specimens were subjected to five levels of compressive logarithmic strains (ε_c): 0% (starting material) and 2%, 4%, 6%, and 8% along the RD. A universal testing machine (Technograph TG-50kN; MinebeaMitsumi Co. Ltd., Japan) and an in-house manufactured die were employed for these tests, as shown in Fig. 3. Additionally, the specimens were annealed at 250 °C for 1 h to mitigate the work hardening caused by the in-plane compression.

Figure 4 presents a schematic of the compression test conducted on the outermost specimen to evaluate its drawability, wherein the circumferential strain $\varepsilon_\theta = |\ln(D/D_0)|$ and thickness direction strain $\varepsilon_t = |\ln(t/t_0)|$ were employed. The diameter of the specimen (D_0) and sheet thickness (t_0) before the test were 28 and 1 mm, respectively, with those after the test denoted as D and t, respectively. A 350-kN universal-sheet metal testing machine (SAS-350D; Tokyo Koki Testing Machine Co., Ltd.) was used, with the punch speed set to 10 mm/min. Additionally, the JIS Z 2249 Type 17 conical cup test die employed used in this experiment. No lubrication was used to ensure that the punch could hold the material. The testing tools and their specifications are listed in Table 1.

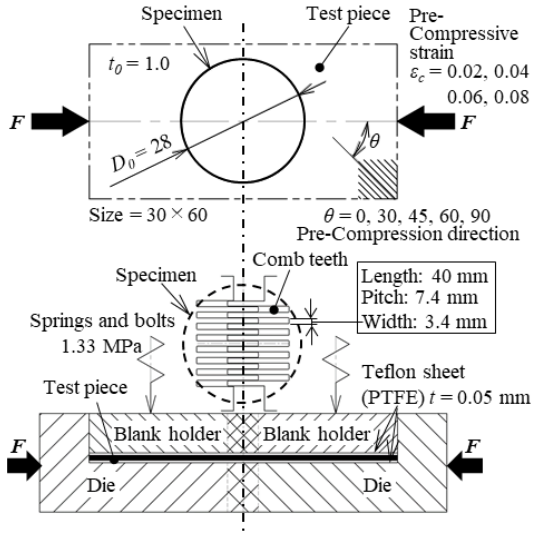

Fig. 2. Schematic of the test specimen and in-plane compression apparatus.

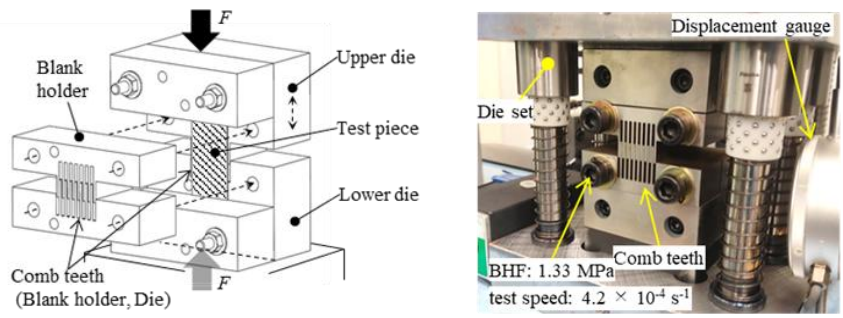

(a) Schematic of the apparatus (b) Photograph of the in-house die assembly

Fig. 3. Schematic and photograph of the apparatus used for in-plane compression. BHF: blank holder force.

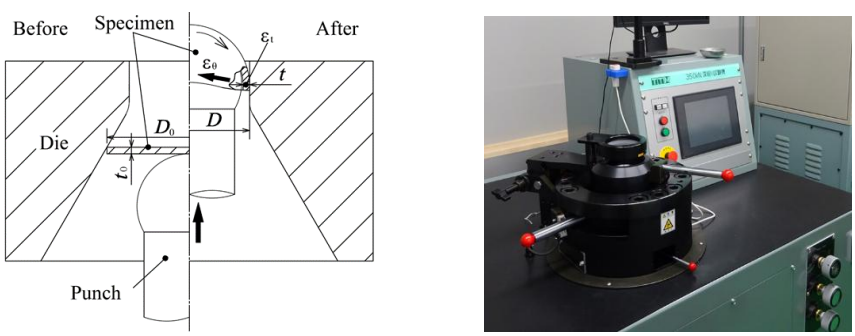

(a) Schematic of compression test of the outermost specimen. (b) Photograph of compression tester.

Fig. 4. Outermost compression-test setup.

Table 1: Testing tools and their specifications (JIS Z2249).

Type	17 type
Die-opening angle	60.00°
Die-hole diameter	19.95 mm
Die-shoulder radius	4.0 mm
Punch diameter (d_1)	17.46 mm
Steel-ball radius	d_1/2 mm

3. Results and Discussion

3.1 Effects of compression direction on formability

Figure 5(a) shows the results of the compression direction (θ) (indicated by the horizontal axis) on the circumferential strain (ε_θ) and thickness strain (ε_t) (represented by the vertical axis) at the fracture point of the outermost specimen. The white and gray bars indicate compressive strains (ε_c) of 0.06 and 0.08, respectively, while the error bars denote the maximum and minimum values (N = 5). The results demonstrate that higher circumferential strain corresponds to improve formability. Additionally, the in-plane compression enhanced formability under all conditions, with the greatest improvement observed at a maximum ε_θ of 0.227 with ε_c= 0.06 and compression direction = 0°. Furthermore, formability ceased to improve from approximately 60°, suggesting that in-plane compression at θ = 0° has a more significant impact on formability than at θ = 90°. A similar trend was observed for thickness strain (ε_t), although the differences with θ were more pronounced, and ε_t noticeably decreased at a compressive pre-strain (ε_c) of 0.08. Moreover, ε_θ remained relatively constant from 0° to 45° as ε_c changed, while ε_t exhibited clear changes. As shown in Fig. 4(a), the outermost layer was constrained by the die in the circumferential direction during testing, limiting its ability to deform freely. This is because the sheet can deform relatively freely in the thickness direction if clearance is present between the specimen and the die, as shown in Fig. 4(a). Therefore, the optimal deformation mode may vary depending on ε_c. Photographs of the fractured test specimens are presented in Fig. 5(b). Evidently, the specimen subjected to ε_c was compressed compared to the test specimen. When ε_c = 0.06 and θ = 60° and 90°, the specimen fractured at the outermost periphery. However, when ε_c = 0.08 and θ = 60° and 90°, the specimen fractured at the punch location due to tension. Additionally, traces of rubbing by the die were observed on the outer peripheries of the specimen. Presumably, a fracture occurs when the outer diameter changes suddenly as the material enters the R-section of the die, as shown in Fig. 4(a). The specimens subjected to ε_c exhibited strong anisotropy, which is evident from the peaks and valleys formed at their outermost peripheries (Fig. 5(b)). Wang et al. [12] conducted uniaxial tensile tests using various compressive pre-strains and compression directions of 0° and 90°, finding that the mechanical responses of specimens cut parallel to and along the compression directions differed. Furthermore, Hama et al. [14] conducted in-plane reversal tests from compression to tension and reported the effects of initial {10-12} twins on the stress–strain relationship. They observed that during the tensile testing, the *r*-value increased as the strain increased.

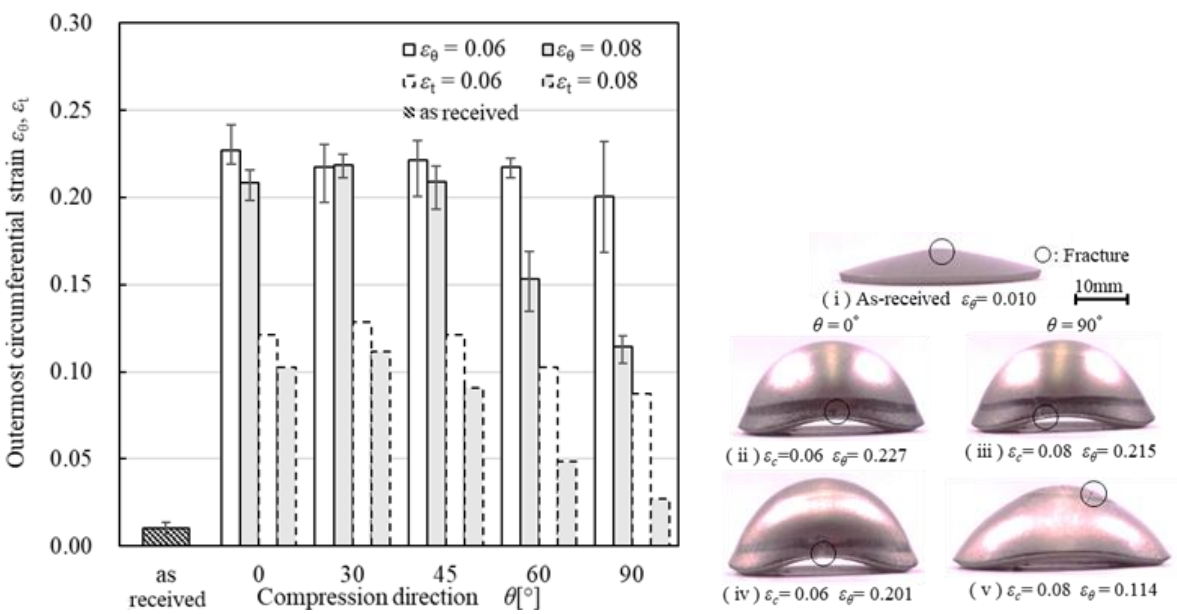

(a) Effects of compression direction on compressive and thickness strains

(b) Specimens after fracturing

Fig. 5. Results of compression strain on the outermost circumferential strain (ε_θ, ε_t) at compression directions of 0–90° and side-views of (i) as-received, (ii) ε_c=0.06, and (iii) ε_c= 0.08 specimens (θ = 0°).

These findings indicate that the material can tolerate greater deformation during the forming process, which is thought to reduce the risk of cracks and defects occurring during forming. This improvement suggests that stable manufacturing is possible for products that require complex shapes and high dimensional accuracy. For example, in cylindrical or disk-shaped parts, increased circumferential strain increases the possibility of realizing thinner walls and lighter weight while maintaining the intended shape. This expands the design freedom of products and is beneficial in terms of reducing material costs and improving energy savings.

Figure 6 shows the (0002) pole figures measured via XRD for compression directions of 0°, 30°, 45°, and 90°. The upper and lower panels depict the (0002) pole figures for compressive strains of $\varepsilon_c = 0.06$ and $\varepsilon_c = 0.08$, respectively, with the basal texture strongly oriented in the compression direction for both strain levels. Additionally, the inclination of the basal texture is higher in the specimen subjected to $\varepsilon_c = 0.08$ (red areas), and the maximum texture strength is significantly decreased to 4.5–7 across all compressive directions. However, the pole figures of the in-plane compressed material indicate that, as the angle increases, the double peak becomes less clear and eventually disappears. The formability under compression directions $\theta = 60°$ and 90° was lower compared to other angles. This difference in formability is believed to stem from differences in the texture orientation relative to the RD, which is influenced by the compression direction. Consequently, it can be concluded that the compression direction plays a crucial role in controlling the orientation of the texture.

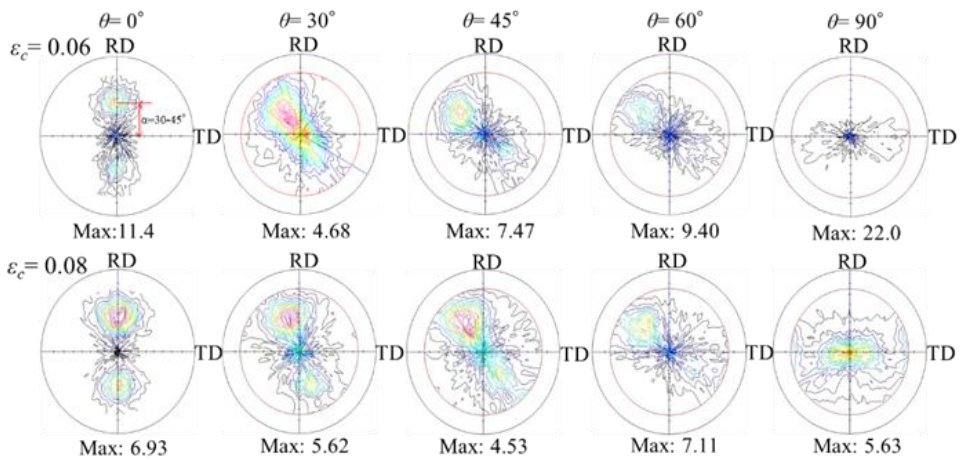

Fig. 6. Effects of compression direction (θ) on the [0002] pole figures of specimens subjected to compressive strains of 0.06 and 0.08.

To explore the relationship between the compressive direction and circumferential strain, as shown in Figs. 5 and 6, the relationship between circumferential strain in each compressive direction and maximum strength was obtained (Figure 7). Evidently, compression directions of 0°–45° resulted in high circumferential strains. However, in some instances, a low ultimate strength and high circumferential strain were observed at a compression direction of 45°. Therefore, no clear correlation was found between the maximum strength (which indicates the basal-texture orientation) and circumferential strain. Nonetheless, a basal-texture orientation concentrated around α = 30°–45° leads to high formability, which remains even if the basal-texture orientation is widely dispersed around this range.

Figure 8 illustrates the relationship between maximum strength and compressive pre-strain (ε_c) for both the basal plane (0002) and the prismatic plane (10-10). The maximum strength of the basal texture (0002) tends to decrease as ε_c increases. At $\varepsilon_c = 0.02$, the strength of the vertical axis of the prismatic plane (10-10) increased by approximately six times compared to the test material and then remained at a roughly constant level. When in-plane compression was applied to the AZ31 Mg-alloy sheet, the basal texture parallel to its surface was weakened, while a columnar texture developed parallel to the sheet surface. Park et al. [13] subjected AZ31 Mg-alloy sheet samples to in-plane compression tests, directly measuring their crystal orientation through EBSD. They reported that {10-12} deformation twins were frequently observed. Therefore, in this test, the occurrence of the {10-12} twin deformation weakened the basal texture parallel to the sheet surface (Fig. 6), and a columnar texture was developed. While the results reported by Park et al. [13] were based on local measurements using EBSD, the XRD results obtained in this study indicate the macroscopic occurrence of {10-12} deformation twins. However, notably, the incomplete pole

figure obtained via XRD showed that the range α = 0°–15° was outside the measurement range. Kim et al. [5] and Park et al. [13], who also performed in-plane compression tests on AZ31 Mg-alloy sheets and directly measured the crystal orientation of the test pieces via EBSD, obtained pole figures indicating that the basal texture (0002) was predominantly oriented in the α = 0°–15° region due to the occurrence of {10-12} twins. Therefore, the basal texture (0002) of this specimen is possibly highly oriented in the α = 0°–15° region. However, XRD did not reveal a basal texture oriented perpendicular to the sheet surface, which was formed by deformation twinning. To precisely evaluate this texture, it is essential to compare it with direct orientation measurements via EBSD.

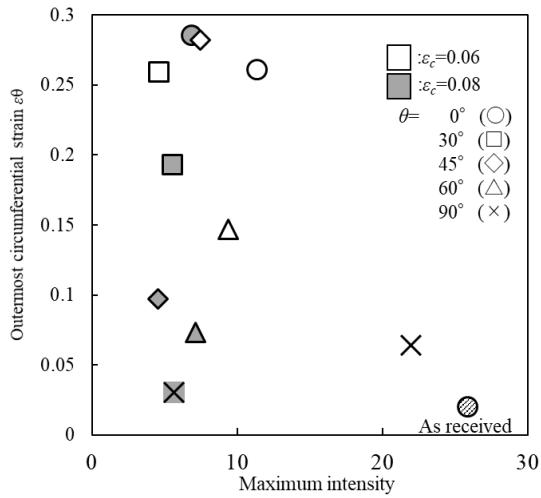

Fig. 7. Relationship between maximum strength and circumferential strain ε_θ.

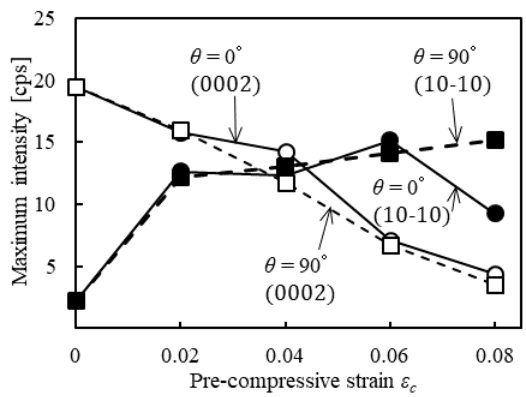

Fig. 8. Relationship between maximum intensity and pre-compressive strain at (0002) and (10-10). Solid and dashed lines show the results for θ= 0° and 90°, respectively.

Figure 9 presents the pole figures of the basal (0002), prismatic (10-10), and tensile-twin {10-12} textures derived via XRD. The pole figure in Fig. 9(a) confirms that the basal textures of the tightly-packed hexagonal crystals are parallel to the RD–TD texture, exhibiting a typical basal texture with a maximum intensity of ≥19. Figures 9(b) and (c) display the pole figures for θ = 0° and 90°, respectively, for ε_c = 0.06 and 0.08. In these figures, the basal textures are oriented parallel to the sheet surface, similar to those of the as-received material, with no significant changes observed. However, the basal texture (0002) of the pole figure for θ = 0° under ε_c = 0.08 is oriented in two directions, approximately 30° from the sheet surface. Additionally, the pole figure for θ = 90° indicates an incomplete separation of a double-peak texture. The slight variation in the shape of the pole figures under the same ε_c suggests that the double-peak texture begins appearing at ε_c = 0.08. This texture resembles those reported by Kohzu et al. [7] and is believed to be closely related to enhanced formability. In a double-peak texture, the texture is divided into two peaks, tilted forward and backward in the compression direction. Notably, alloys have been reported to form under severe conditions close to the fracture limit, such as low temperatures or high reduction ratios. This results in axisymmetric

basal texture that provides excellent low-temperature formability. Furthermore, for the prismatic texture (10-10), pole figures similar to those for the basal texture (0002) were obtained for both $\theta = 0°$ and 90°, with a higher maximum strength, suggesting that the crystal was aligned parallel to the sheet surface. In the tension twin texture {10-12}, the texture, which was circumferentially oriented under both $\theta = 0°$ and 90°, began to orient in a specific direction as the compressive pre-strain increased. This orientation coincided with the direction of the loading axis during the in-plane compression tests. Moreover, the maximum strength of each measurement texture increased slightly with increasing compressive pre-strain [16]. Therefore, an increase in compressive pre-strain may lead to the formation of a texture with a specific orientation. A double-peak texture has been achieved using a rolling technique [7] and repeated bending [10], which typically involve warm processing or multiple processing steps. However, this study demonstrated that a double-peak texture can be easily obtained at room temperature in a single step using an in-plane compression test. We also found that the orientation could be controlled by altering the compression direction. Furthermore, compressive pre-strains of 0.06 and 0.08 are advantageous for improving formability, near the compressive pre-strain ε_c at which the double-peak texture was observed.

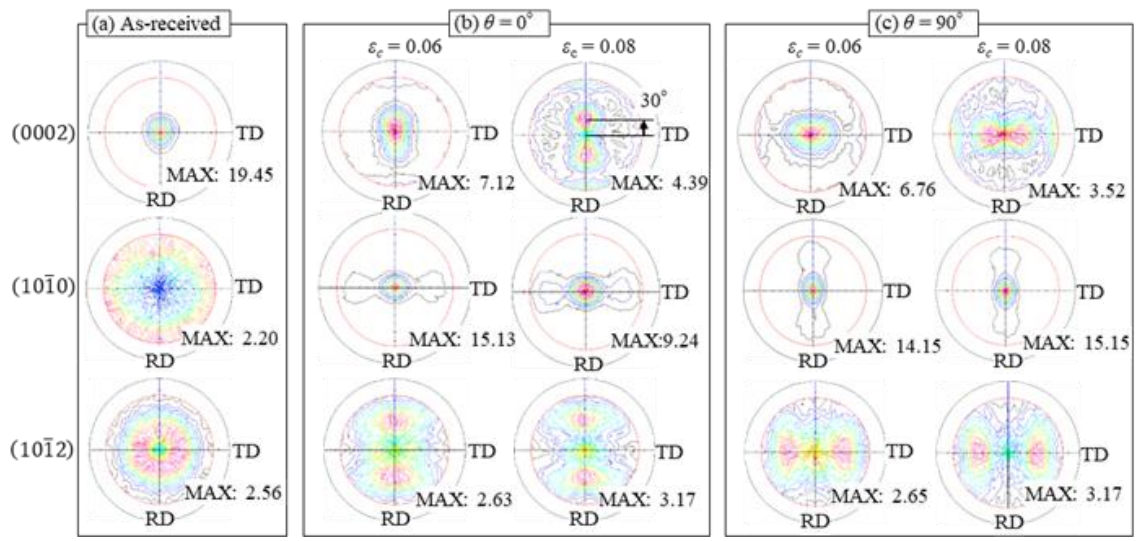

Fig. 9. Pole figures of (0002), (10-10), (10-12) for $\varepsilon_c = 6\%$ and $\varepsilon_c = 8\%$ for (a) as-received, (b) $\theta = 0°$ and (c) $\theta = 90°$ specimens.

3.2 (0001) pole figure representing the hexagonal basal texture

Figure 10 displays the (0001) pole figures (stereographic projections) representing the hexagonal basal planes (hereafter referred to as the basal texture) obtained through EBSD. The centers of the pole figures correspond to the ND axis (normal to the RD–TD plane), while the contours depict the pole-density distributions. The closer the color is to red, the more hexagonally the *c*-axes of the grains are oriented in the same vicinity. That is, the redder the center of the circle, the more the basal texture of each crystal grain is formed parallel to the sheet surface. In the 0% material, a dominant proportion of crystal grains exhibit a hexagonal *c*-axis (hereafter referred to as *c*-axis) orientation that nearly coincides with the ND axis (referred to as tendency ①). In the 2 and 4% materials, some grains appear to rotate approximately 60°–90° toward the RD axis (indicated as tendency ②). In the 6 and 8% materials, tendency ① decreases, while tendency ② increases significantly. Notably, even with an in-plane compressive strain of approximately 8%, which is not considered a large deformation, the texture of the Mg-alloy sheet changes significantly.

In pole-density distributions of the (0001) pole figures, the *c*-axes of each grain were mainly located between 0° and 30° or between 60° and 90° when the ND axis was considered as the reference (0°) (Fig. 10). For simplicity, we defined the inclination-angle range of the *c*-axis as follows: Zone A (0°–30°), Zone B (30°–60°), and Zone C (60°–90°). Figure 11 showcases the relationship between the area ratio of the crystal grains (hereafter referred to as area ratio) and the inclination angle of the *c*-axis for each in-plane compression-test specimen. The plots depict inclination angles of the *c*-axis ranging from 5°–85° in 10° intervals. For example, the area fraction in the range of 0°–9° along

the *c*-axis was evaluated at the 5° position. The 0% material exhibited the highest area ratio for Zone A, which then decreased significantly from Zone B to Zone C. In contrast, the 8% material exhibited a significantly higher area ratio for Zone C. The results for all the other conditions fell between those of the 0 and 8% materials. These results are consistent with those reported by Kim et al. [5], who conducted a similar verification, indicating that there were no issues with the machining accuracy of in-plane compression-test specimens.

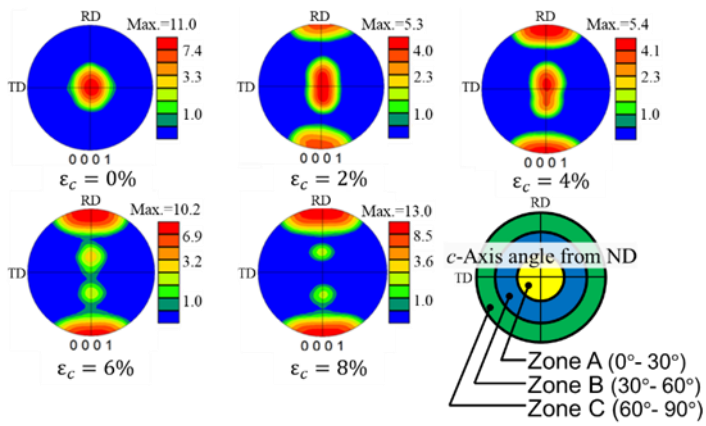

Fig. 10. (0001) pole figures (stereographic projections) obtained via EBSD showing the hexagonal basal texture.

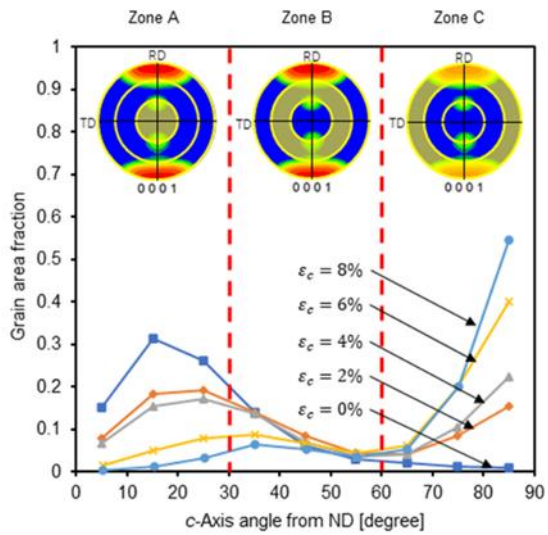

Fig. 11. Relationship between grain-area fraction and crystal orientation.

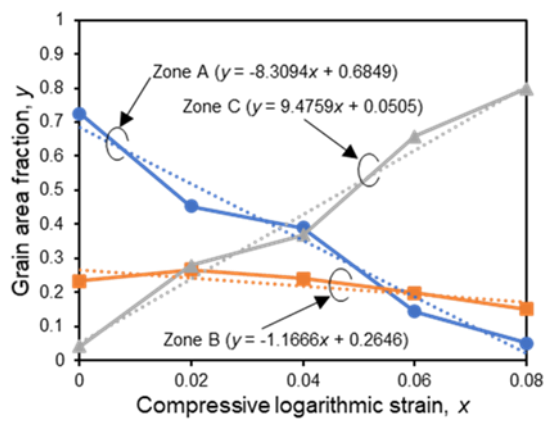

Fig. 12. Relationship between the area ratios and in-plane compressive strain in each zone.

The relationship between the area ratio and in-plane compressive strain in each zone was determined from the results shown in Fig. 11, with the outcomes of the first-order approximation presented in Fig. 12. In Zone A, the maximum and minimum area fractions of the in-plane compressive strains were 0 and 8%, respectively, while in Zone C, these values were reversed at 8 and 0%, respectively. The median area fraction for both zones was 4%, indicating a linear relationship between the decreasing (Zone A) and increasing (Zone C) in-plane compressive strains. The overall area ratio of Zone B remained approximately 20%, which can be considered roughly stable. Comparisons of the absolute slope values of each approximation equation showed no significant differences between the Zones A and C. However, the slope value for Zone B was considerably lower. This suggests that in-plane compression rotates the grains whose *c*-axes are located in Zones A and C but does not affect the rotation in Zone B [17]. Additionally, the primary active slip/twin system of Mg at room temperature is the {10-12} tension twin, followed by the basal texture [18]. It has been suggested that this system is activated when subjected to tensile deformation along the *c*-axis (equivalent to compressive deformation perpendicular to the *c*-axis), causing the *c*-axis to rotate by approximately 86°. In this study, most of the grains with *c*-axes in Zone A transformed into Zone C via in-plane compression, which was close to the *c*-axis rotation angle owing to the {10-12} tension twinning. Therefore, the texture formed by applying in-plane compression to Mg-alloy sheets is considered to be predominantly influenced by the {10-12} tension twins.

4. Conclusion

This study confirmed the enhancement of the formability of rolled AZ31B Mg-alloy sheets by analyzing the circumferential strain under each compression direction and compression strain. However, the formability in compression directions of 60° and 90° was lower compared to other directions. Observations of the test specimens following the outermost-layer compression test revealed strong in-plane anisotropy, as evidenced by peaks and valleys at the outermost peripheries of the samples subjected to compressive strain. This strong anisotropy, along with the variation in formability based on compression direction, is consistent with the texture orientation in the load-axis direction (as previously reported by Wang et al. [12] and Hama et al. [14]). The circumferential strain under compression directions of 0°-45° remained relatively unchanged despite variations in the compressive pre-strain, while changes in the thickness strain were more pronounced. This suggests that the favourable deformation mode may shift if the compressive strain changes. At a compressive strain of 0.08, the basal texture (0002) exhibited a double peak, which is considered advantageous for improving formability. Furthermore, a texture that contributed to improving the formability beyond that of the double-peak texture was obtained at a compressive strain of 0.06. Additionally, pole figure observations of the of the basal (0002) and prismatic (10-10) faces indicated the occurrence of {10-12} twins. This activation enhances the material's capacity for deformation, as it allows for more slip directions to accommodate stress. Consequently, this shift improves the material's ductility, allowing it to undergo larger strains without fracturing. These findings suggest that a compressive pre-strain of 0.06 and a compression direction of 0° are optimal for achieving a texture that improves the formability of rolled AZ31B Mg-alloy sheets.

Nomenclature

θ	compression direction
ε_θ	circumferential strain
ε_t	thickness strain
ε_c	compressive pre-strain
EBSD	Electron backscattered diffraction
RD	rolling direction
TD	transverse direction
XRD	X-ray diffraction

References

[1] Chino Y, Huang X, Saito N, Nishiwaki T, Mohri T, Matsuda M. Effects of process parameters on room-temperature deep drawability of AZ31B magnesium alloy sheets with suppressed basal texture. Journal of the Japan Society for Technology of Plasticity (JSTP). 2023;64(744):13–18.

[2] Chino Y, Mabuchi M, Kishihara R, Hosokawa H, Yamada Y, Wen C, Shimojima K, Iwasaki H. Mechanical properties and press formability at room temperature of AZ31 Mg alloy processed by single roller drive rolling. Materials Transactions. 2002;43(10):2554–2560.

[3] Sunaga Y, Tanaka Y, Asakawa M, Katoh M, Kobayashi M. Effect of twin formation by repetitive bending on texture of AZ61 magnesium alloy sheet and improvement of formability. Journal of the Japan Institute of Light Metals (Keikinzoku). 2009;59(12):655–658.
[4] Nishino S. Press forming technology of magnesium alloy sheets. Journal of the Japan Institute of Light Metals (Keikinzoku). 2011;61(6):269–273.
[5] Kim S-J, Lee C, Koo J, Lee J, Lee Y-S, Kim D. Improving the room-temperature formability of a magnesium alloy sheet by texture control. Materials Science and Engineering A. 2018;724:156–163.
[6] Park SH, Lee JH, Huh Y-H, Hong S-G. Enhancing the effect of texture control using {10-12} twins by retarding detwinning activity in rolled Mg–3Al–1Zn alloy. Scripta Materialia. 2013;69(11):797–800.
[7] Kohzu M, Kii K, Nagata Y, Nishio H, Higashi K, Inoue H. Texture randomization of AZ31 magnesium alloy sheet for improvement of cold formability by combination of rolling and high temperature annealing. Journal of the Japan Institute of Light Metals (Keikinzoku). 2010;60(5):237–243.
[8] Yamamoto A, Terashita M, Tsubakino H. Textures in AMCa602 and AZ31B magnesium alloys formed by wavy bend pressing. Journal of the Japan Institute of Light Metals (Keikinzoku). 2007;57(3):99–104.
[9] Okawa M, Mori S, Hiyokawa K, Fujii N, Murakami T, Takasaki A. Improvement of room-temperature formability of rolled AZ31B magnesium alloy sheets by in-plane compression and subsequent heat treatment. Journal of the Japan Society for Technology of Plasticity (JSTP). 2019;60(706):315–320.
[10] Noguchi T, Suzuki K, Huang X, Saito N, Tsukada Y, Koyama T, Chino Y. Effects of bending and tension deformation on texture evolution and room temperature formability of AZ31B alloy sheets. Journal of the Japan Institute of Metals and Materials. 2019;83(6):212–220.
[11] Okawa M, Mori S, Murakami T, Takasaki A. Relation between flange fracture and blankholder force in the process of cylindrical deep drawing of AZ31B rolled magnesium alloy sheets. Journal of the Japan Institute of Light Metals (Keikinzoku). 2019;69(2):113–119.
[12] Wang L, Cao M, Cheng W, Zhang H, Cao X, Mostaed E. Improved stretch formability of AZ31 magnesium thin sheet by induced {10-12} tension twins. JOM. 2018;70(10):2321–2326.
[13] Park SH, Hong S-G, Lee CS. Enhanced stretch formability of rolled Mg–3Al–1Zn alloy at room temperature by initial {10-12} twins. Materials Science and Engineering A. 2013;578:271–276.
[14] Hama T, Suzuki T, Hatakeyama S, Fujimoto H, Takuda H. Role of twinning on the stress and strain behaviors during reverse loading in rolled magnesium alloy sheets. Materials Science and Engineering A. 2018;725:8–18.
[15] Kuwabara T, Kumano Y, Ziegelheim J, Kurosaki I. Tension–compression asymmetry of phosphor bronze for electronic parts and its effect on bending behavior. International Journal of Plasticity. 2009;25(9):1759–1776.
[16] Katahira T, Hosokawa S, Naka T, Kohzu M, Adachi H, Yoshida F. Effect of temperature on cyclic plastic deformation of AZ31 Mg alloy sheet. Journal of the Japan Society for Technology of Plasticity. 2016;57(661):135–139.
[17] Kelley EW, Hosford W. Plane-strain compression of magnesium and magnesium alloy crystals. Transactions of the Metallurgical Society of AIME. 1968;242(1):5–13.
[18] Partridge PG. The crystallography and deformation modes of hexagonal close-packed metals. Metallurgical Reviews. 1967;12(1):169–194.